

The LCO/Palomar 10,000 km s^{-1} Cluster Survey. I. Properties of the Tully-Fisher Relation

Jeffrey A. Willick¹

Department of Physics, Stanford University, Stanford, CA 94305-4060

ABSTRACT

The first results from a Tully-Fisher (TF) survey of cluster galaxies are presented. The galaxies are drawn from fifteen Abell clusters that lie in the redshift range ~ 9000 – $12,000$ km s^{-1} and are distributed uniformly around the celestial sky. The data set consists of R -band CCD photometry and long-slit $\text{H}\alpha$ spectroscopy. The rotation curves (RCs) are characterized by two parameters, a turnover radius r_t and an asymptotic velocity v_a , while the surface brightness profiles are characterized in terms of an effective exponential surface brightness I_e and scale length r_e . The TF scatter is minimized when the rotation velocity is measured at $r = (2.0 \pm 0.2)r_e$; a significantly larger scatter results when the rotation velocity is evaluated at $\gtrsim 3$ or $\lesssim 1.5$ scale lengths. This effect demonstrates that RCs do not have a universal form, specified only by luminosity, as suggested by Persic, Salucci, & Stel. The scatter minimum at $r = 2r_e$ is interpreted in terms of a thin stellar disk plus spherical dark halo mass model. Variations in halo mass and size at fixed disk mass and size can produce extra TF scatter at arbitrary radii, but no additional scatter at the special radius $r = 2r_e$ provided $\rho_h \propto M_h^{-0.7}$. In contrast to previous studies, a modest but statistically significant surface-brightness dependence of the TF relation is found, $v \propto L^{0.28} I_e^{0.14}$. This indicates a stronger parallel between the TF relation and the corresponding Fundamental Plane relations of elliptical galaxies than has previously been recognized. The scatter of the optimized TF relation decreases with increasing luminosity and surface brightness, from ~ 0.75 mag for low-luminosity, low-SB objects to $\lesssim 0.35$ mag for high-luminosity, high-SB objects. This effect is well described by a model in which the intrinsic TF scatter is ~ 0.30 mag, and most of the remaining scatter is caused by rotation velocity measurement errors of ~ 15 km s^{-1} independent of rotation amplitude. Future papers in this series will consider the implications of this cluster sample for deviations from uniform Hubble flow on $\gtrsim 100h^{-1}$ Mpc scales.

¹Cottrell Scholar of Research Corporation. Email: jeffw@perseus.stanford.edu

1. Introduction

In the late 1980s and early 1990s, several groups reported the existence of large-scale bulk flows in the local universe (Dressler *et al.* 1987; Willick 1991; Mathewson, Ford, & Buchhorn 1992; Han & Mould 1992; Courteau *et al.* 1993; Lauer & Postman 1994; recent reviews of the subject include Dekel 1994, Postman 1995, Strauss & Willick 1995, and Strauss 1997). These studies suggested that high-amplitude ($v_p \gtrsim 500 \text{ km s}^{-1}$) peculiar velocities might be coherent across large volumes, tens to perhaps hundreds of megaparsecs in diameter. The actual coherence scale of the flows has been poorly constrained, however. The results of Lauer & Postman, in particular, suggested that this scale could be as large as $300h^{-1} \text{ Mpc}$. Other, more recent, studies (e.g. Giovanelli *et al.* 1996; Riess *et al.* 1997) have indicated a much more modest coherence scale for bulk flows, $\lesssim 50h^{-1} \text{ Mpc}$.

The question of the coherence scale for high-amplitude bulk flows is an important one for cosmology, because this scale is sensitive to the underlying power spectrum of density fluctuations. In most models of large-scale structure formation, one does not expect Lauer-Postman like flows (see, e.g., Strauss *et al.* 1995). To address the question of the bulk flow coherence scale, the author undertook a Tully-Fisher (TF) and Fundamental Plane (FP) survey of cluster galaxies beginning in 1992. The observations for this survey (§3) were carried out from the Las Campanas (LCO) and Palomar Observatories, and the cluster sample was restricted to a narrow range of redshifts near $cz = 10,000 \text{ km s}^{-1}$. For this reason, the survey is referred to as the LCO/Palomar $10,000 \text{ km s}^{-1}$ Cluster Survey (LP10K). Observations and analysis of the TF data have recently been completed, and the first results are reported here. A second paper (Willick 1998a, Paper II) will discuss constraints on bulk flows from the LP10K TF data set, and a third paper will present the TF data (Willick 1998b, Paper III). The FP survey is ongoing, with results expected in 2–3 years.

The focus of the present paper is on the form of the TF relation that emerges from the LP10K data set. Originally, TF studies used photoelectric apparent magnitudes and 21 cm velocity widths. Thus, the data per galaxy were limited. The LP10K TF survey is one of a number of recent TF surveys in which CCD surface photometry is combined with long-slit optical spectroscopy. The information per galaxy is thus considerably increased relative to the original TF surveys, and the implications of these additional data are only now being fully appreciated. A key goal of this paper is to explore how to make optimal use of the full range of photometric and spectroscopic data in applying the TF relation.

The outline of this paper is as follows. § 2 provides a brief overview of the key issues involved in analyzing TF data, and discusses the significance of these issues for our understanding of galaxy structure. §§ 3 and 4 describe the observations and data reduction for the LP10K survey. § 5 presents the TF fitting procedure and results. § 6 presents an inter-

pretation of the key features of the TF relation in terms of galaxy structure. § 7 summarizes the main points of the paper.

2. The TF Relation

The relationship between spiral galaxy luminosity and rotation velocity (the TF relation) was first noted by Tully & Fisher (1977). They and subsequent workers in the 1970s and 1980s measured rotation velocity from the width of the 21 cm line (see, e.g., Aaronson *et al.* 1982, 1986; Botinelli *et al.* 1983; Pierce & Tully 1988). During this period few TF studies made explicit use of the fact that, in reality, spirals do not have a single, well-defined rotation velocity, but rather exhibit a *rotation curve* (RC), $v_c(r)$, where r is distance from the galaxy center. However, the fact that many spirals exhibit “flat” RCs (e.g., Rubin *et al.* 1982), in which $v_c(r)$ rises rapidly from zero at the center and then is constant to the largest observed radii, suggested that the 21 cm width did indeed reflect a well-defined quantity: “the” rotation velocity—i.e., the velocity of the flat part of the RC—of the galaxy.

In the late 1980s and early 1990s, several new TF surveys substituted, in whole or in part, long-slit optical spectroscopy for 21 cm velocity width measurement. Courteau (1992, 1997) analyzed over 300 Northern sky Sb-Sc galaxies using *R*-band photometry and long-slit spectra. Courteau (1997; see also Courteau & Rix 1999) showed that this data set produced an optimized TF relation when the velocity was measured from the RC at 2.2 exponential disk scale lengths. Mathewson, Ford, & Buchorn (1992) carried out a TF study of over 1300 Southern sky objects, of which about half had optically measured RCs. This subset was reanalyzed by Kasen (1997) who found an optimized TF relation when the rotation velocity was measured at a radius encompassing 83% of the total light of the galaxy. Schlegel (1995) conducted a TF survey of IRAS galaxies and found an optimized TF relation for $v_c(r)$ evaluated at an isophotal radius. Simon (1998) analyzed a 95-galaxy subset of the SHELLFLOW sample (Courteau *et al.* 1998) and found a minimum TF scatter when the the rotation velocity was measured at 1.7 disk scale lengths.

While differing in detail, the above studies all demonstrated that there is no unique, *a priori* TF rotation velocity for spirals with carefully measured RCs. In particular, they agreed that fitting the observed RCs and using the asymptotic rotation velocity, the amplitude of the flat portion of the RC, does not yield an optimized TF relation. Rather, the RC amplitude must be evaluated at a radius determined from the photometric properties of the galaxy. A corollary is that even galaxies whose RCs never “turn over”—are still rising even at the outermost radii observed—can be assigned rotation velocities that fit the TF relation. The analysis presented here will confirm and extend these conclusions. These issues are important

not only for applying the TF relation, but also for understanding spiral galaxy structure, because the radius at which velocity best correlates with luminosity is a function of the relative distribution of dark and luminous matter (Courteau & Rix 1999; McGaugh & de Blok 1998; Navarro 1998).

A second element of recent TF surveys has been accurate CCD surface photometry. Thus, not only apparent magnitudes, but well-defined surface brightnesses, radii, and luminosity shape parameters are available for all galaxies. In principle, this photometric information allows the incorporation of additional parameters into the TF relation. However, efforts to find such parameters have not yielded fruit in the past (Han 1991; Willick 1991). The picture that has emerged has been of the TF relation as a two-parameter (one-dimensional) relation between rotation velocity and luminosity only. This picture contrasts with that which has emerged for elliptical galaxies over the last decade (e.g., Djorgovski & Davis 1987; Bender, Burstein & Faber 1992; Jorgensen *et al.* 1996). Ellipticals exhibit a three-parameter relation between luminous radius, surface brightness, and velocity dispersion known as the Fundamental Plane (FP). This has led to the question of why ellipticals and spirals differ in this regard. An important conclusion of this paper will be that spirals in fact exhibit properties more similar to ellipticals than previously suspected; when properly analyzed the TF relation is a three-parameter one similar to the FP.

3. Observations and Preliminary Data Reductions

The observations were carried out during the period 1992–1995 at the Las Campanas Observatory (LCO) in Chile and at Palomar Observatory in California. Fifteen Abell Clusters were selected as target fields from which the galaxy samples were to be selected. They are shown in Table 1. The selection criteria were (1) published cluster redshifts in the range $0.03–0.04$ ($9000 \leq cz \leq 12,000 \text{ km s}^{-1}$), (2) an approximately isotropic, full-sky distribution, and (3) Galactic latitude $|b| \geq 20^\circ$. The last criterion was imposed to minimize the effects of Galactic extinction. In practice, a large number of Abell clusters with $0.03 \leq z \leq 0.04$ was identified, and 15 were selected from among them in such a way as to achieve the greatest degree of isotropy.

The observational strategy was as follows. *R*-band CCD imaging of wide ($\sim 1–2$ square degree) fields centered on each cluster was carried out from the LCO 1 m and Palomar 1.5 m telescopes. Approximately 25 contiguous frames, each consisting of 2 or 3 exposures totalling 15 minutes (LCO) or 10 minutes (Palomar), were taken in each cluster. The CCD frames were

TABLE 1
 LCO/PALOMAR CLUSTER SAMPLE

Abell #	RA (1950)	DEC (1950)	z	R ^a	m_{10}^b
Las Campanas Clusters ^c :					
2731	0 07.7	-57 16	.0312	0	15.3
3381	6 08.1	-33 35	.0382	1	14.7
3202	3 59.0	-53 48	.0388	1	15.8
0496	4 31.3	-13 21	.0320	1	15.3
1139	10 55.5	1 46	.0383	0	15.0
3578	13 54.7	-24 29	.0400	1	15.1
3733	20 59.0	-28 15	.0386	1	15.6
3869	22 18.2	-55 23	.0396	0	15.3
2657	23 42.3	8 52	.0400	1	14.9
Palomar Clusters ^d :					
0260	1 49.0	32 55	.0348	1	15.8
0576	7 17.3	55 50	.0381	1	14.4
1228	11 18.8	34 36	.0350	1	13.8
2199	16 26.9	39 38	.0300	2	13.9
2247	16 52.0	81 39	.0384	0	15.3

Table 1: Notes: (a) Abell Richness class. (b) Photographic magnitude of the 10th brightest cluster member. (c) Clusters observed primarily or exclusively from LCO. (d) Clusters observed primarily or exclusively from Palomar.

bias-corrected, flatfielded, registered and coadded using standard procedures within IRAF². Automated galaxy identification using the FOCAS package (Jarvis & Tyson 1981) was then done, and all objects brighter than $m_R \simeq 17$ and minor-to-major axis ratios $b/a \gtrsim 0.2$ were visually inspected. From these a subsample whose appearance indicated relatively late-type (\gtrsim Sb) morphology was selected for follow-up long-slit spectroscopy. The morphology cut was found to be critical for maintaining a high H α detection rate. The precise magnitude limit varied from cluster to cluster, because an effort was made to obtain 15–20 TF data points per cluster, which occasionally required observations of galaxies as faint as $m_R \simeq 18$.

²IRAF is distributed by the National Optical Astronomy Observatories, which are operated by the Association of Universities for Research in Astronomy, Inc., under cooperative agreement with the National Science Foundation.

In addition to the cluster images, standard star fields from the compilation of Landolt (1992) were multiply observed on each LCO 1 m and Palomar 1.5 m night deemed photometric, providing zero points for the R band galaxy photometry.

The long-slit spectroscopy was conducted from the LCO 2.5 m and Palomar 5 m telescopes at a resolution of ~ 1 Å/pixel. The slit was oriented along the major axis of the galaxy as determined from the CCD images. The wavelength coverage was ~ 6200 –7200 Å, allowing detection of $\text{H}\alpha$ out to a redshift of $z \simeq 0.1$. Exposure times ranged from 10–45 minutes (see below). The 2-dimensional spectrograms were flat-fielded, rectified, and wavelength-calibrated using standard IRAF procedures. Measurement of a rotation curve (RC) was possible only when extended emission lines were detected, about 50–60% of all exposures. Another $\sim 10\%$ of exposures yielded nuclear emission that sufficed for redshift determination but not RC measurement. In virtually all cases $\text{H}\alpha$ was the strongest emission line seen and was the only one used to trace the RC. In a handful of cases a cosmic ray or chip flaw compromised $\text{H}\alpha$ and made it necessary to use the N[II] or S[II] lines to trace the RC.

Two unexpected factors complicated the observational program. First, the rate of detection of $\text{H}\alpha$ was considerably lower than anticipated. To minimize waste of large-telescope time, a strategy was adopted in which short exposures (5–10 minutes) were taken, the result inspected for $\text{H}\alpha$, and a longer frame taken only if $\text{H}\alpha$ was detected in the short frame and deemed likely to produce a usable RC. The relatively low $\text{H}\alpha$ detection rate also meant that more candidates than expected had to be observed in order to obtain the hoped-for number of detections. Accordingly, the long exposures themselves, initially 45 minutes in length, were shortened to 20–30 minutes beginning in 1993. Moreover, the $\text{H}\alpha$ detection rate varied significantly from cluster to cluster. The original plan called for ~ 15 TF objects per cluster. In practice, the number varies from as few as 8 objects to as many as 23 objects with TF data in the different clusters. These differences reflect the fact that in some clusters the $\text{H}\alpha$ detection rate was over 90%, while in others it was $\lesssim 30\%$.

The second unanticipated complication was the prevalence of background objects in many of the clusters. The reason for drawing the galaxy sample from cluster fields was to ensure that a narrow redshift range around $10,000$ km s $^{-1}$ was sampled. It turned out, however, that in some of these fields many galaxies did not lie at the published cluster redshift. In Abell 3733 (published redshift $cz = 11,600$ km s $^{-1}$), for example, the *majority* of the final TF sample objects have $cz \geq 20,000$ km s $^{-1}$. Similar though less extreme results were found in a number of other clusters, especially those in the Southern celestial sky (the reason for this is unknown and may be worth further investigation). In the final TF sample only about two-thirds of the objects have redshifts $7000 \leq cz \leq 15,000$ km s $^{-1}$, which might

be called the extended target range. The remaining 1/3 almost all have $15,000 \leq cz \leq 30,000 \text{ km s}^{-1}$, with only a handful of foreground ($cz \leq 7000 \text{ km s}^{-1}$) galaxies. Although this fact reduces the sensitivity of the survey to the bulk flow of a $10,000 \text{ km s}^{-1}$ shell, it does not compromise the purposes of the present paper which are simply to explore the TF relation.

4. Production of the Final Data Set

4.1. Derivation of Photometric Parameters

The images of galaxies with emission lines in the long-slit spectra were subjected to further analysis using the VISTA image-processing package (Stover 1988; see Willick 1991 or Courteau 1992 for a detailed discussion of spiral galaxy surface photometry using VISTA). Elliptical isophotes were fitted to the high to moderate S/N portion of the galaxy images. The fitted ellipses which best matched the galaxy disk were visually identified and were taken to define the global ellipticity ($\varepsilon \equiv 1 - b/a$) and position angle (PA) of the galaxy. The surface brightness profile was then extended to a final radius, r_f , within ellipses of this fixed shape and orientation. Aperture magnitudes were also computed, via direct summation of pixel values, within these fixed ellipses out to r_f . The value of r_f was determined by the requirement that the galaxy surface brightness at this radius equal the uncertainty in the sky background determination.

The surface brightness profile was extrapolated beyond r_f by fitting an exponential function, $I(r) = I_0 e^{-r/r_d}$, to the outer portion of the measured profile. It was usually not appropriate to fit the entire profile because of manifestly nonexponential features such as a strong central bulge. The fit parameters I_0 and r_d , while not necessarily characteristic of the entire profile, were thus suitable for calculating the luminosity extrapolation,

$$\Delta L = 2\pi(1 - \varepsilon)I_0 r_d^2 e^{-r_f/r_d} \left[1 + \frac{r_f}{r_d} \right], \quad (1)$$

which was added to the aperture magnitude within r_f to obtain the “total” magnitude of the galaxy, later used in the TF analysis. Typical extrapolations via this method were 0.03–0.10 mag.

The fit parameters I_0 and r_d , while suitable for the luminosity extrapolation, were not found to be the optimal measures of SB and radius for the TF analysis; as noted above, these parameters were often not characteristic of the bright inner parts of the galaxy. An alternative procedure for determining a characteristic surface brightness I_e and scale r_e was therefore developed. The details are somewhat technical and are presented in Appendix A.

Here we note only that (1) I_e and r_e are determined from the intensity moments of the galaxy, not from any kind of parametric fit, and thus are robust and objective, and (2) I_e and r_e are defined in such a way that they agree with the exponential disk parameters I_0 and r_d if the entire surface brightness profile is well described by an exponential law. Thus, I_e and r_e are an “effective” exponential surface brightness and scale length, but they are not predicated on the galaxy’s actually having an exponential profile. Their value as characteristic parameters is best justified a posteriori from their role in defining the TF relation (§5).

A final photometric parameter that proved useful was the *luminosity concentration index* c , defined by

$$c \equiv 5 \log \frac{r_{60}}{r_{20}} \quad (2)$$

where r_X is the radius containing $X\%$ of the total light.

4.2. Derivation of Spectroscopic Parameters

The two-dimensional wavelength-calibrated spectrograms were interactively processed to extract the RC. Full details of the procedure are given by Simon (1998). Briefly, following sky-subtraction, the approximate position of the $\text{H}\alpha$ emission was interactively marked out along the slit. Accurate central wavelengths were then found as a function of position, with spatial averaging done in regions of low S/N. The galaxy center was computed by finding the centroid of the continuum longward and shortward of $\text{H}\alpha$ and averaging. A rotation curve was then obtained by applying the Doppler shift formula and subtracting the velocity corresponding to the position of the galaxy center, which was taken as the systemic redshift of the galaxy.

The full RCs contain a significant amount of information, not all of which can be used in the TF analysis. It was thus decided to fit each RC with a simple function that would encompass its key features. A suitable choice is a two-parameter arctangent fit,

$$v_c(r) = \frac{2v_a}{\pi} \tan^{-1} \left(\frac{r}{r_t} \right), \quad (3)$$

which was found to provide a reasonable fit to the RC in all cases³. In Equation (3), v_a represents the asymptotic or “flat” value of the RC, while r_t is a “turnover” radius where the RC reaches one-half its asymptotic value, roughly separating the linear and flat part of

³In practice, a four-parameter fit was carried out, in which the galaxy center and the mean radial velocity were allowed to vary from their initial estimates obtained from the spectrogram processing. In general, the refinements of the central position and velocity were quite small.

the RC. It is important to note that v_a is a fit parameter and not the actual asymptotic value of the RC, which, indeed, was not observed in many cases because the RC was still rising at the last observed radius. The arctangent fit is above all a convenient interpolation formula for determining the amplitude of the RC at any chosen radius, as discussed in the next section.

4.3. Corrections to the Raw Data

The procedures above yield the basic observational data for each galaxy:

1. The kinematic data: heliocentric redshift cz_\odot (km s^{-1}) and RC parameters v_a (km s^{-1}) and r_t (arcsec).
2. The photometric data: total magnitude m_R (R -band magnitudes) and effective surface brightness μ_e (R -band magnitudes per square arcsecond, the magnitude equivalent of I_e ; cf. §4.1), characteristic radius r_e (arcsec), concentration index c , and ellipticity $\varepsilon = 1 - b/a$.

Prior to fitting the TF relation several standard corrections were applied. The heliocentric redshift cz_\odot was converted to a microwave background frame (CMB) redshift, henceforward denoted cz with no subscript. The galaxy inclination was computed from the ellipticity as described by Willick *et al.* (1997a). The asymptotic velocity v_a was corrected for inclination and redshift broadening. The effective surface brightness μ_e was corrected for $(1 + z)^4$ cosmological dimming. The total magnitude was corrected for Galactic extinction, internal extinction, and cosmological effects following Willick *et al.* (1997a), with two key differences. First, the coefficient of $\log(a/b)$ used in the internal extinction correction was 1.20, somewhat higher than the value of 0.95 used by Willick *et al.* The higher value was chosen to eliminate any trends of the TF residuals with axial ratio, and may result from the fact that R band magnitudes have a shorter effective wavelength than the r band magnitudes used by Willick *et al.* Second, the extinction maps of Schlegel *et al.* (1998), which are based on IRAS/DIRBE maps of dust emission, were used in preference to Burstein-Heiles extinctions. The corrected total magnitudes are denoted m with no subscript.

An additional inclination correction was required for the surface brightness. The values of μ_e corrected only for cosmological dimming exhibited a significant correlation with axial ratio. This trend was removed by computing corrected effective surface brightnesses $\mu_e^{(c)} = \mu_e - 0.85 \log(a/b)$. The corrected values of μ_e are used in the remainder of this paper.

5. Modelling the TF Relation

5.1. Sample Definition

The total LP10K TF sample, meaning all objects with both photometric and RC data, numbers 268 distinct galaxies. About fifty of these galaxies have multiple (2–4) photometric measurements, and about thirty have two RC measurements. (A detailed accounting will be provided in Paper III.) For the purposes of the TF analysis, we will consider as “objects” *all photometry/spectroscopy data point pairs for a given galaxy*. Thus, for example, if a galaxy has two RC measurements and two photometric ones, it contributes four objects to the analysis. The effect of this on the statistical significance of the results is discussed below.

The multiplicity of photometry and spectroscopy is such that the 268 galaxies yield 386 objects. To improve reliability we further pruned the sample as follows: (i) We required $\log(a/b) \geq 0.06$ to exclude objects that are too face-on. (ii) We excluded objects with absolute magnitudes (based on a Hubble flow distance model, see below) fainter than $-18.5 + 5 \log h$ (galaxies fainter than this were consistently poor fits to the TF relation). (iii) Objects with purely linear RCs—for which the arctan fit constrained only the ratio v_a/r_t , not either parameter separately—were excluded. (iv) Objects whose RCs exhibited no perceptible width were excluded. (v) One galaxy with $cz < 2000 \text{ km s}^{-1}$ was excluded. These cuts eliminated 34 objects, leaving a full TF sample of 352 objects, comprising 245 distinct galaxies.

The fact that a significant fraction of the sample has multiple measurements reduces the number of statistical degrees of freedom for the analysis. Normally, a sample of N data points and p free parameters has $N - p$ degrees of freedom. This would still be the case here if the TF scatter arose entirely from observational errors, because then different measurements of an individual galaxy would be statistically independent. However, as will be shown below, a significant portion of the TF scatter is intrinsic. As a result, the TF errors of two or more data points corresponding to an individual galaxy are strongly correlated.

A full discussion of this difficult issue will be deferred to Paper II. For the present we take a conservative approach and simply assume that the effective number of independent data points is simply the number of distinct galaxies in the sample, 245. The actual number is larger, because the observational scatter arises largely from the velocity width measurement, so we could arguably count the same galaxy twice if it has two measured RCs. Moreover, the different photometric measurements of a given object, while they yield similar apparent magnitudes, produce somewhat different measures of inclination and scale length which yield different velocity widths even for a single RC. However, the conservative approach suffices here because the effects considered in this section have high statistical significance, and slight

underestimates of their significance are thus unimportant.

In what follows we use a likelihood analysis to study the properties of the TF relation. The likelihood statistic \mathcal{L} we define in §5.4 has the property that, if the data points entering into it are independent, a decrease of one unit, over and above degrees of freedom added, corresponds to a one-sigma likelihood increase; an increase of four units over and above the added degrees of freedom corresponds to a two-sigma likelihood increase (cf. Willick *et al.* 1997b for a more detailed discussion). To correct for the nonindependence of the data points, we scale the statistic by a factor $N_{indep}/N_{tot} \approx 245/352 = 0.696$. This scaling ensures that the above rules for assessing the significance of changes in \mathcal{L} continue to hold, and we use these rules in the discussion to follow.

5.2. Distance Assignments

To fit the TF relation distances must be assigned to each galaxy from redshift-space information. The LP10K TF sample consists, in principle, of cluster galaxies, and the members of a given cluster are often assumed to lie at a common distance. However, for a variety of reasons this “cluster paradigm” (Willick *et al.* 1995) is a poor approximation here. As already noted, one-third of the sample consists of background galaxies with redshifts as high as $z = 0.1$. Applying the cluster paradigm would require a careful pruning of objects using distinct redshift limits for each cluster, which in the end would be rather arbitrary. Moreover, the true redshifts of the clusters are not necessarily well known. In addition, many sample spirals come from the outskirts of the clusters rather than from their presumably virialized cores. Finally, Willick *et al.* (1995) found, in any case, that the redshift-distance relation for cluster spirals was often better approximated by Hubble flow than by the cluster paradigm in any case.

For the above reasons, we assign distances (in Mpc) to all galaxies using a simple Hubble-flow model,

$$d = H_0^{-1}cz, \quad (4)$$

where for definiteness we take $H_0 = 65 \text{ km s}^{-1} \text{ Mpc}^{-1}$. (Uncertainty in the Hubble constant translates directly into errors in the TF zero point derived from the analysis, but does not affect any other relevant parameters.) Modifications of this distance law for possible bulk flows, as well a careful division between cluster and non-cluster galaxies, will be considered in Paper II. These considerations have no meaningful effect on the properties of the TF relation itself, however.

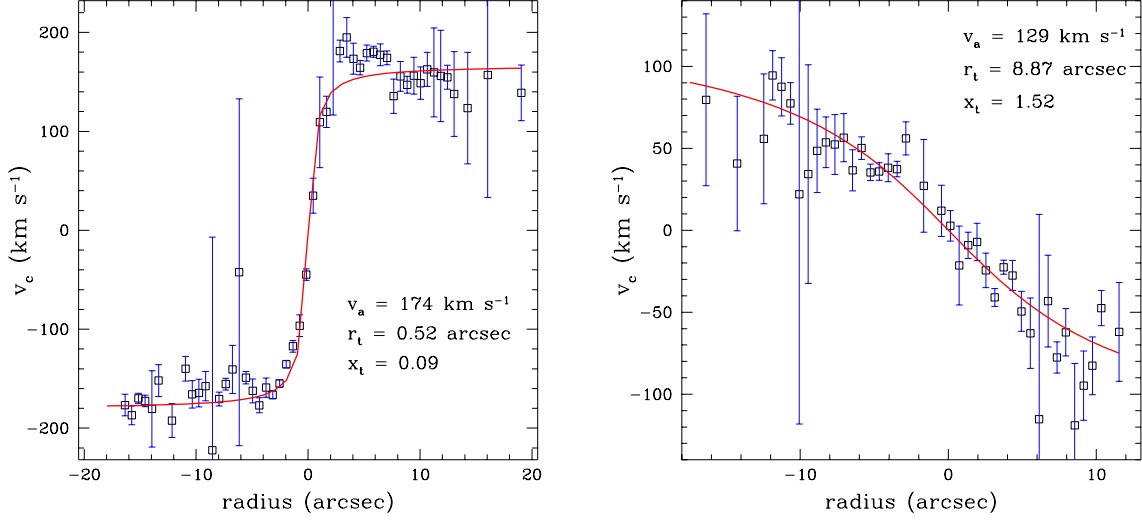


Fig. 1.— Two representative rotation curves from the LP10K sample. Both are from the cluster A2199. The left hand panel shows a galaxy with a classical flat RC, and with $x_t \ll 1$. The right hand panel shows a galaxy with a slowly rising RC, in which the asymptotic velocity is not reached in the observed region. Correspondingly, it has $x_t > 1$. See text for further details.

5.3. Parameterization of the TF Relation

Throughout this paper, we use the “inverse” form of the TF relation (Strauss & Willick 1995, §6.1) in order to minimize selection bias effects. We define the “circular velocity parameter”

$$\eta \equiv \log (2v_{\text{TF}}) - 2.5, \quad (5)$$

where v_{TF} is the measure of rotation velocity that optimizes the TF relation (see below). The inverse TF relation is then written, in its simplest, two-parameter form, as

$$\eta = -e(M - D), \quad (6)$$

where M is absolute magnitude, and e and D are the inverse TF slope and zero point.

We follow Courteau (1997) in supposing that v_{TF} is obtained by evaluating the fitted RC at a multiple of the characteristic radius of the galaxy. Here, however, we use the effective exponential radius r_e rather than the fitted exponential scale length (cf. §4.1). Thus,

$$v_{\text{TF}} = \frac{2v_a}{\pi} \tan^{-1} \left(\frac{f_s r_e}{r_t} \right), \quad (7)$$

where we treat f_s as a free parameter to be determined by optimizing the TF relation. It will prove useful to define a dimensionless parameter

$$x_t = \frac{r_t}{r_e}, \quad (8)$$

a ratio of dynamical to luminous scale length. In terms of x_t we write the TF rotation velocity as

$$v_{\text{TF}} = \frac{2v_a}{\pi} \tan^{-1} \left(\frac{f_s}{x_t} \right). \quad (9)$$

The value of the x_t parameter can best be appreciated from representative RC plots, as shown in Figure 1. Because galaxy rotation is typically detected out to $\sim 3\text{--}5 r_e$, the value of x_t determines whether the curve exhibits a classical flat shape ($x_t \ll 1$), or whether the RC is still rising at the outermost observed radii ($x_t \gtrsim 1$). Hence, x_t is basically an RC shape parameter. We will make further use of this below.

5.4. Method of Fit

We adopt a maximum likelihood approach for determining the TF parameters. The method is based on the VELMOD likelihood approximation outlined by Willick & Strauss (1998; cf. Appendix 1 of that paper). The observed values of η are assumed to be normally distributed about their predicted values,

$$P(\eta_i|m_i, cz_i) = \frac{1}{\sqrt{2\pi}\sigma_{\text{eff},i}} \exp \left\{ -\frac{(\eta_i - [-e(m_i - 5 \log d_i - 25 - D)])^2}{2\sigma_{\text{eff},i}^2} \right\}. \quad (10)$$

In Eq. 10 σ_{eff} is the effective TF scatter given by

$$\sigma_{\text{eff},i}^2 = \sigma_\eta^2 + \left(\frac{5e}{\ln 10} \frac{\sigma_v}{d_i} \right)^2 \quad (11)$$

where σ_η is the inverse TF scatter (intrinsic plus observational errors), and σ_v is the velocity dispersion relative to Hubble flow. We treat σ_η as a free parameter, but fix σ_v at 250 km s^{-1} . The sample is too distant to reliably determine σ_v (cf. the discussion by Willick *et al.* 1997b). The likelihood for observing the entire data set is $\mathcal{P} = \prod_i P(\eta_i|m_i, cz_i)$, where the product runs over all data points. We maximize this likelihood by minimizing $\mathcal{L} \equiv -2 \ln \mathcal{P}$ with respect to the various free parameters.

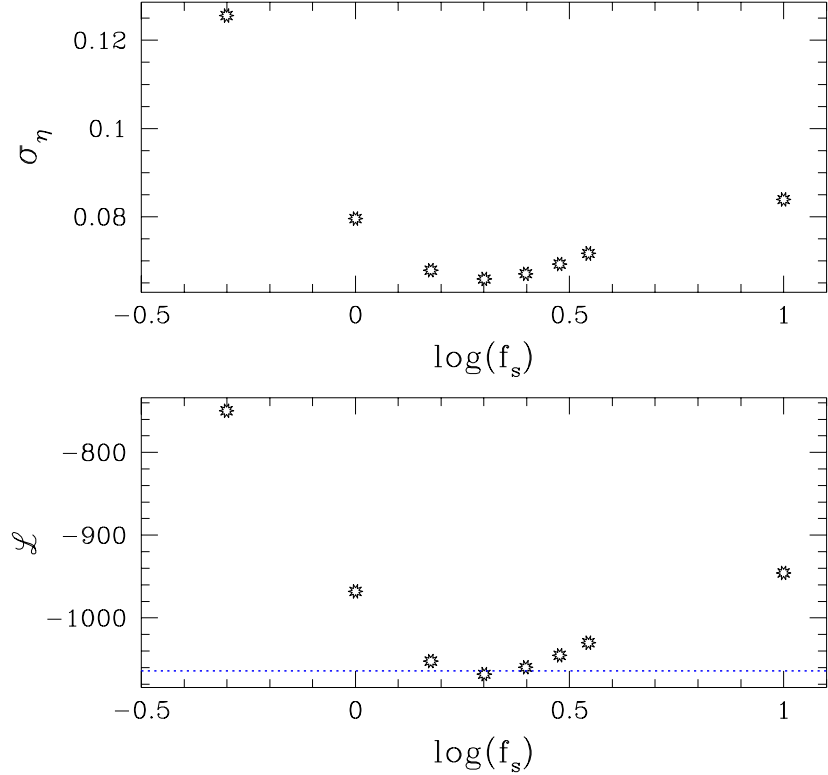


Fig. 2.— Inverse TF scatter (top panel) and the fit likelihood statistic \mathcal{L} (bottom panel) for a two parameter (rotation velocity-luminosity) TF fit, plotted against $\log f_s$, where f_s is the parameter that determined the radius at which v_{TF} is evaluated (see equation 7 and the surrounding text for details). A strong minimum in TF scatter, and a corresponding maximum in fit likelihood, are seen at $f_s = 2.1$. The dotted line in the lower panel shows indicates $\Delta\mathcal{L} = 4.0$ relative to the minimum of \mathcal{L} , corresponding to the 2- σ confidence limits on the value of f_s .

5.5. Establishing the value of f_s

The free parameters appearing explicitly in the model (equation 10) at this point are D , e , and σ_η . In subsequent sections, we will treat f_s , and other parameters not yet introduced, as free parameters. Before doing so, however, it is useful to maximize likelihood with respect to changes only in the zero point, slope, and scatter of the TF relation, for a range of fixed values of f_s . This exercise will demonstrate the presence of a strong minimum in the TF scatter for $f_s \approx 2$, a result that will prove robust to the introduction of additional free parameters.

In Figure 2, the TF scatter σ_η and the corresponding value of \mathcal{L} are plotted versus $\log f_s$ for a sequence of fits done at fixed values of f_s . Both σ_η and \mathcal{L} are minimized (likelihood is maximized) for $f_s = 2.0 \pm 0.2$ (one-sigma errors; the corresponding two-sigma, determined by the dotted line in the lower panel, are $\sim \pm 0.35$). Values of $f_s \lesssim 1.5$ and $f_s \gtrsim 3$ are strongly ruled out. Note, in particular, that the TF scatter is much larger, and the likelihood of the fit vastly smaller, for very large ($\gtrsim 10$) f_s , which corresponds to using the asymptotic flat portion of the RC as the TF rotation velocity. We conclude that there exists a characteristic radius, ~ 2 effective exponential scale lengths, at which rotation velocity correlates most strongly with luminosity. This conclusion is consistent with those reached by Courteau (1997), Kasen (1997), and Simon (1998).

5.6. SB/Concentration Dependence of the TF Relation

The maximum likelihood values of D , e , σ_η , and f_s , for the two-parameter, rotation velocity-luminosity TF relation are given in the first row of Table 2. (Note that fitting the two-parameter TF relation involves four free parameters, because f_s and σ_η also are varied.) In Figure 3 inverse TF residuals, $\eta(\text{observed}) - \eta(\text{predicted})$, from this fit are plotted versus surface brightness (top panel) and concentration index (lower panel). A mild but significant trend is can be seen with respect to surface brightness. The diagonal line of slope 0.05 indicates the approximate slope of this trend. A weaker trend is seen in the residual versus concentration index plot, though it appears to be significant only for the most concentrated galaxies ($c \gtrsim 3$).

These trends show that the two-parameter TF relation does not adequately describe the data. We improve it by writing the TF relation in the following, four-parameter form:

$$\eta = -e(M - D) - \alpha(\mu_e - 19.2) + \beta(c - 2). \quad (12)$$

(We normalize μ_e and c to typical values so as to minimize changes in the TF zero point.) The second and third rows of Table 2 show the results of incorporating first μ_e and then both μ_e and c into the TF relation. With each added free parameter, the likelihood is significantly improved (see the discussion in §5.1). In particular, incorporating μ_e results in a 21 unit decrease of \mathcal{L} , a $\sqrt{(21 - 1)} \simeq 4.5$ -sigma likelihood increase. Thus, the surface brightness dependence of the TF relation is highly statistically significant, although the maximum likelihood value of $\alpha \simeq 0.05$ is not especially large, corresponding to $v_{\text{TF}} \propto I_e^{0.13}$. The likelihood improvement when concentration index is incorporated into the fit is smaller, but still significant at the 3σ level. Note that this improvement occurs *after* SB has been added to the fit; thus, the SB- and concentration index-dependences of the TF relation are

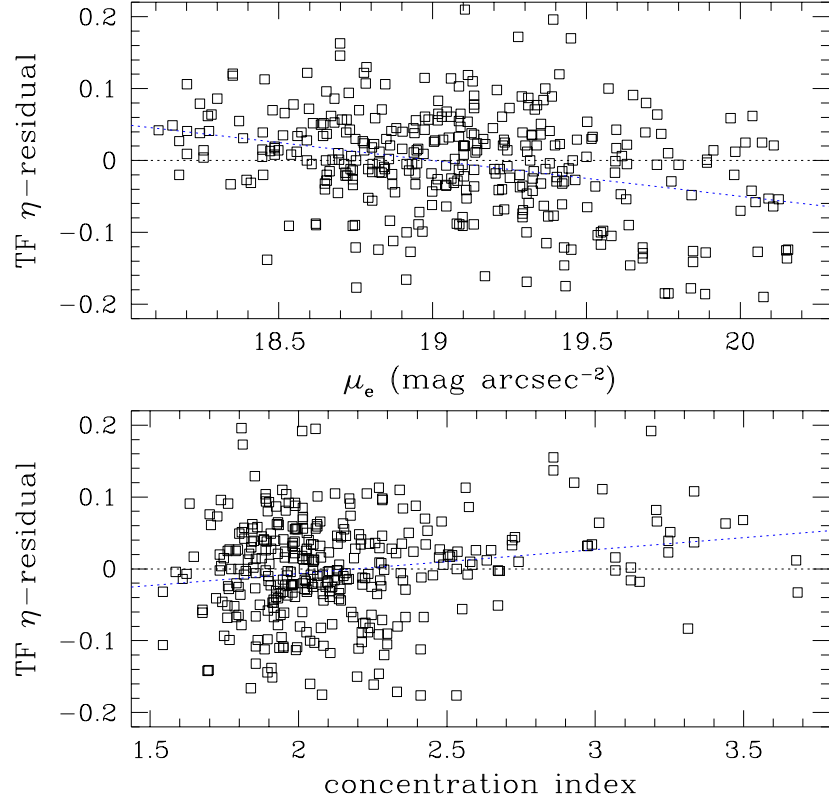


Fig. 3.— Inverse TF residuals from a standard 2-parameter (rotation velocity-luminosity) TF fit are plotted against surface brightness μ_e (upper panel) and concentration index c (lower panel). in the top panel. The diagonal lines indicate the approximate slopes, 0.05 for μ_e and 0.04 for c . The trends are significant at the $\sim 4.5\sigma$ level for μ_e and at the $\sim 3\sigma$ level for c (see text), indicating that the TF relation depends on both of these parameters.

distinct from one another. Residuals with respect to μ_e and c from the four-parameter TF relation, with the parameters given in the third row of Table 2, are shown in Figure 4. No trends can be seen, indicating that equation 12 is an acceptable description of the TF relation. Note that although f_s was treated as a free parameter when fitting equation 12, its maximum likelihood value was virtually unchanged from the two-parameter fit (compare the values of f_s listed in rows 1–3 of Table 2).

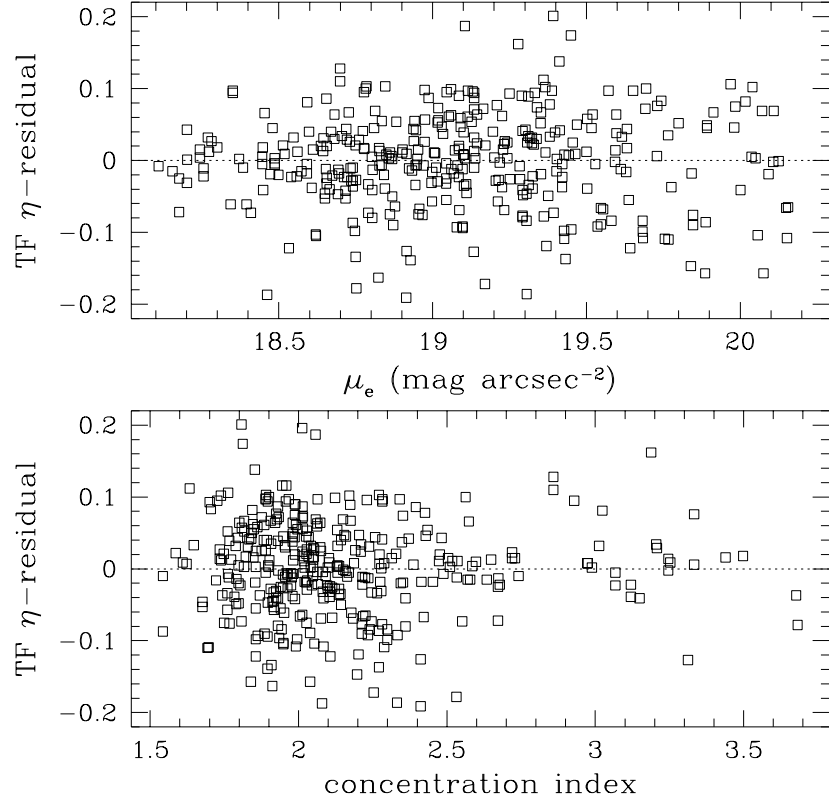


Fig. 4.— Same as the previous figure, except that now the residuals for a four-parameter TF fit (equation 12) are shown. No trends are evident.

5.7. Luminosity-Dependence of the TF Scatter

Fitting the four-parameter TF relation involved six free parameters: the four in Eq. 12, plus σ_η and f_s . A significant improvement in the likelihood can be achieved with the addition of a seventh parameter that describes the decrease in TF scatter for higher luminosity, higher surface brightness galaxies. Such a scatter decrease was detected for certain low-redshift TF samples by Willick *et al.* (1997a,b) and by Willick & Strauss (1998). Here, however, the effect is even stronger, as can be seen in Figure 5, in which TF residuals are plotted versus luminosity for the six-parameter fit. Low-luminosity galaxies exhibit larger residuals, in the mean, than do high-luminosity objects. We follow Willick & Strauss (1998) and write $\sigma_\eta = \sigma_{\eta,0} + g_i(M - \bar{M})$ where \bar{M} is the mean absolute magnitude of the sample (-21.48 for the LP10K sample). When g_i was included as the seventh free parameter in the fit, a 13.2-unit decrease in \mathcal{L} relative to the six-parameter fit was achieved, a 3.2σ improvement. The best-fit result was $g_i = 0.011$, more than twice as large as the value found by Strauss &

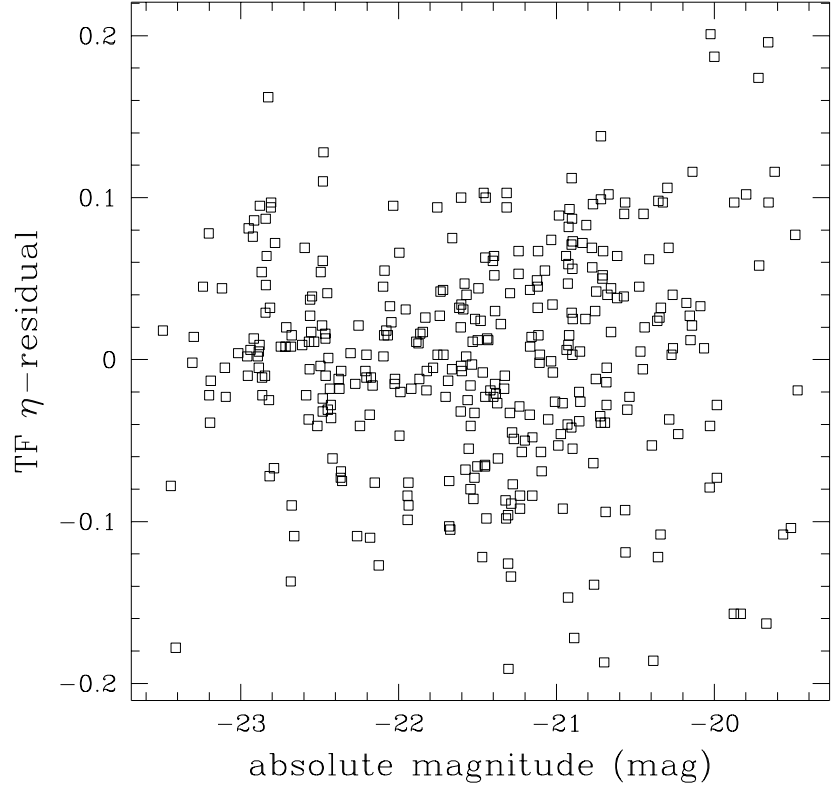


Fig. 5.— Inverse TF residuals from the four-parameter TF fit, equation 12, plotted versus luminosity. It can be seen that low-luminosity galaxies exhibit larger TF scatter than high-luminosity ones.

Willick (1998) for the MAT sample. Thus, TF scatter decreases by $\sim 20\%$ for each magnitude of luminosity.

However, luminosity alone may not be the sole indicator of TF scatter. For example, in the upper panel of Figure 4 we see that scatter also correlates with surface brightness, in the sense that higher-SB galaxies appear to have smaller TF scatter. We can describe this effect with a linear model as well, and find a similar likelihood increase as we did in the previous paragraph.

TF scatter thus decreases with increasing luminosity and with increasing surface brightness. Each effect alone is about equally significant. This suggests that the underlying factor is that the scatter decrease is most strongly correlated with increasing v_{TF} itself. Such an effect indeed has a natural physical explanation. Suppose that one makes, on average, a constant error δv_{TF} in measuring the rotation velocity (including errors in the inclination

TABLE 2
TF FIT PARAMETERS: f_s -FORMULATION^{a,b}

D	e	α	β	f_s	σ_η	δv_{TF}^c	\mathcal{L}^d	Notes
–21.619	0.1314	–	–	1.994	0.0659	–	–1068.1	e,f,g
–21.657	0.1216	0.0467	–	2.033	0.0631	–	–1089.3	f,g
–21.765	0.1102	0.0533	0.0454	1.957	0.0617	–	–1100.0	g
–21.758	0.1122	0.0589	0.0450	2.001	0.0366	15.95	–1116.8	h

Table 2: Notes: (a) The parameters D , e , α , and β are defined by equation 12. σ_η is the overall inverse TF scatter, except as noted in the fourth row of the table. (b) The TF rotation velocity is defined according to equation 9, i.e., it is the rotation velocity evaluated from the arctan fit to the RC at f_s times the effective exponential scale radius r_e . f_s is treated as a free parameter, and its maximum-likelihood value is listed. (c) The mean rotation velocity measurement error, in km s^{-1} , as determined from maximum likelihood via equation 14. (d) The likelihood statistic is scaled by the ratio of the number of independent (245) to total (352) data points in the fit (see §5.1). (e) SB dependence of the TF relation not modeled. (f) Concentration-index dependence of the TF relation not modeled. (g) σ_η treated as a constant in fit. (h) Overall TF scatter modeled according to equation 14. The listed value of σ_η actually represents the quantity σ_0 in that equation.

correction). The corresponding error in the circular velocity parameter is

$$\delta\eta = \frac{1}{\ln 10} \frac{\delta v_{\text{TF}}}{v_{\text{TF}}} = 0.055 10^{-\eta} \frac{\delta v_{\text{TF}}}{20 \text{ km s}^{-1}}, \quad (13)$$

where in the last step the definition of η has been explicitly taken into account. A reasonable model is then to assume that the total TF scatter consists of an η -independent portion (intrinsic scatter plus photometric and distance assignment errors), σ_0 plus the error specified by equation 13, added in quadrature:

$$\sigma_\eta = \sqrt{\sigma_0^2 + \left[0.055 \frac{\delta v_{\text{TF}}}{20}\right]^2 10^{-2\eta(M, \mu_e, c)}}. \quad (14)$$

(Note that in evaluating σ_η one uses not the observed but the predicted η in the exponent, as we are doing an inverse fit.)

A fit using equation 14 for σ_η produced a greater likelihood increase than either a luminosity- or an SB-dependent scatter alone. The maximum-likelihood parameters resulting from such a fit are given in the fourth row of Table 2. The likelihood statistic changed by about 17 units with the addition of a single free parameter, δv_{TF} , a four-sigma improvement. Combined with its having a reasonable physical motivation, this likelihood increase leads us to adopt equation 14 as a meaningful description of the TF scatter.

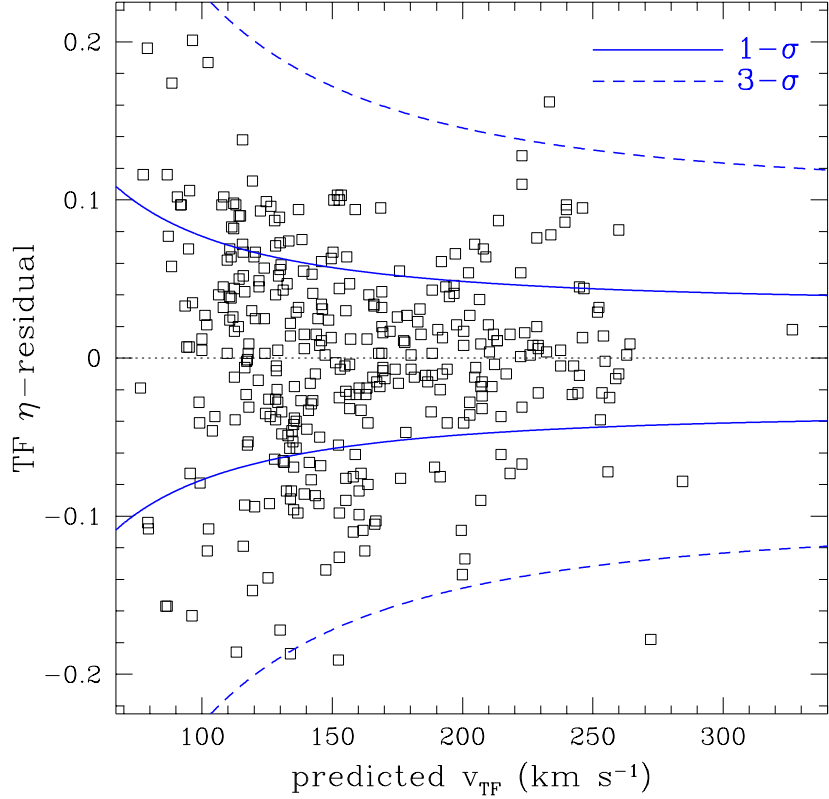


Fig. 6.— Inverse TF residuals plotted against the predicted TF velocity, v_{TF} , based on the four parameter fit. The solid lines indicate the 1σ , and the dashed lines the 3σ , predictions based on equation 14. With the exception of a larger-than expected number of 3σ deviations, equation 14 gives a good account of the observed TF scatter. See text for details.

The maximum likelihood values of the scatter parameters are $\sigma_0 = 0.036$ (corresponding to ~ 0.30 mag), and $\delta v_{\text{TF}} = 15.6 \text{ km s}^{-1}$. The latter is a reasonable value for a typical rotation velocity measurement error. Figure 6 shows TF residuals plotted versus $v_{\text{TF}}(\text{predicted}) = 158.1 \times 10^{\eta(M, \mu_e, c)} \text{ km s}^{-1}$. Overplotted are the values of σ_η and $3\sigma_\eta$ as predicted from equation 14. The model provides a reasonable description of the observed TF residuals. The one way in which it breaks down is that there are more 3σ deviant points than one would expect from Gaussian statistics. This may point less to a failure of this particular model of the scatter, but instead to the general non-Gaussianity seen in many TF samples (Willick *et al.* 1996), in the sense that a few percent of any given sample is likely to exhibit large residuals. The remainder of the points are, to a good approximation, Gaussian.

The curves in Figure 6 show that velocity width measurement errors dominate the

TF scatter for slow rotators ($v_{\text{TF}} \lesssim 150 \text{ km s}^{-1}$), while for rapid rotators, $v_{\text{TF}} \gtrsim 200 \text{ km s}^{-1}$, i.e., high-luminosity, high SB galaxies, the constant error term, σ_0 , dominates. This error, as noted above, includes photometric and distance errors, plus intrinsic scatter. Because the former are quite small in general ($\lesssim 0.1$ mag), the value of σ_0 is largely indicative of the intrinsic scatter of the TF relation. Our result here thus implies that the intrinsic TF scatter is $\lesssim 0.30$ mag, a result obtained through entirely independent means by Willick *et al.* (1996). The overall scatter within the observed range of v_{TF} ranges from about $\sigma_\eta \approx 0.085$ for $v_{\text{TF}} \approx 100 \text{ km s}^{-1}$ to $\sigma_\eta = \sigma_0 = 0.037$ for $v_{\text{TF}} \gtrsim 300 \text{ km s}^{-1}$. Given the inverse TF slope of $e = 0.112$, these values correspond to equivalent forward TF scatter values of 0.33–0.75 mag. This large range helps explain why different samples have yielded different values of the TF scatter in the past (cf. the discussion by Willick 1998c).

5.8. An Alternative Formulation of the TF Relation

The TF relation, equation 12, explicitly contains four parameters (e , D , α , β), but implicitly a fifth parameter, f_s , is present in the definition of v_{TF} and thus η . An equivalent approach is to make the fifth parameter explicit, as follows. First, we let $\eta_a \equiv \log(2v_a) - 2.5$, i.e., we take the asymptotic velocity from the arctan fit as the TF rotation velocity. Then we make x_t an explicit parameter in the TF relation:

$$\eta_a = -e(M - D) - \alpha(\mu_e - 19.2) + \beta(c - 2) + \gamma x_t. \quad (15)$$

To fit this TF relation to the LP10K data set we must first prune the sample a bit further by requiring $x_t < 2$. For $x_t > 2$ the RCs are very nearly linear and v_a is highly uncertain (recall that purely linear RCs had already been eliminated). The resultant sample consists of 341 data points comprising 237 distinct galaxies.

Figure 7 shows TF residuals [now defined as $\eta_a(\text{observed}) - \eta_a(\text{predicted})$] from equation 15 as a function of x_t . In the top panel, residuals resulting from a four-parameter fit, with $\gamma \equiv 0$, are shown, while in the bottom panel residuals from the five-parameter fit (with the best-fit value of γ indicated) are plotted. In each case, the scatter model given by equation 14 was used, with δv_{TF} held fixed at 15.95 km s^{-1} to facilitate comparison with the f_s -formulation. The maximum-likelihood parameters for the two fits are listed in Table 3. A strong trend with x_t is obvious in the upper plot; the lower plot shows no trend, indicating that a the linear model is a good one. The statistic \mathcal{L} decreases by 132 units when x_t is included in the fit, a huge likelihood increase.

These results show that when x_t is not taken into account ($\gamma \equiv 0$), luminosity is a poor predictor of v_a . Galaxies with slowly rising rotation curves ($x_t \gtrsim 1$) have a much larger

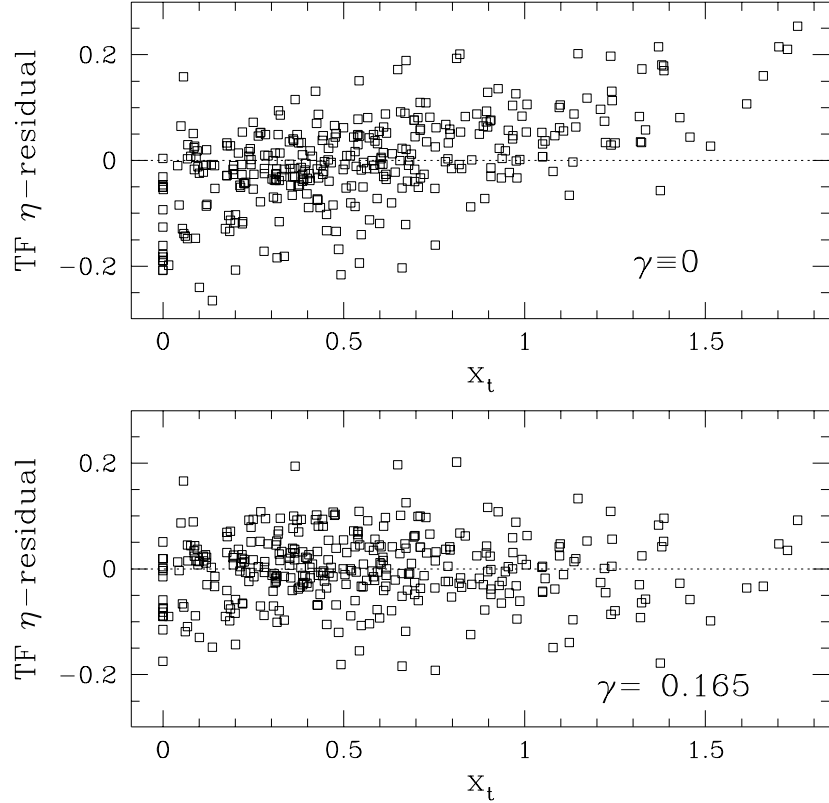


Fig. 7.— Inverse TF residuals from the five-parameter TF fit, equation 15, plotted as a function of the RC shape parameter x_t . In the top panel the coefficient of x_t in the fit, γ , has been fixed at zero. When this is done, a strong trend of residuals with x_t is evident, and the corresponding TF scatter is very large ($\sigma_\eta \simeq 0.079$). In the bottom panel, γ was varied to produce the maximum likelihood fit. No trend of the residuals are now evident, indicating that when x_t is included in the TF fit, the asymptotic RC amplitude v_a can be effectively used in the TF relation.

asymptotic RC amplitude than their luminous mass suggests. The term $0.165x_t$ corrects this deficit: luminosity (along with SB and concentration), *in combination with* x_t , predicts the asymptotic RC amplitude well. Indeed, the TF scatter and likelihood for the fit based on Eq. 15 are nominally better than (though statistically equivalent to) those obtained from a fit based on Eq. 12, the f_s -formulation, for the same 341-galaxy sample.

The explicitly five-parameter TF relation is useful because it clarifies why a TF relation based on v_a and luminosity (with or without SB and concentration) is a very poor one: *galaxies of a given luminosity can have very different RC shapes*, as determined by x_t . Figure 8, in which x_t is plotted against absolute magnitude (left panel) and surface brightness (right

TABLE 3
TF FIT PARAMETERS: x_t -FORMULATION^{a,b}

D	e	α	β	γ	σ_0^c	δv_{TF}	\mathcal{L}^d	Notes
–21.834	0.0881	0.0767	0.0104	–	0.0650	15.95	–958.3	e,f
–21.808	0.1173	0.0551	0.0406	0.165	0.0347	15.95	–1090.7	f

Table 3: Notes: (a) The parameters D , e , α , β , and γ are defined by equation 15. (b) The TF rotation velocity is taken to be the asymptotic value, v_a . The RC shape parameter x_t now enters explicitly into the TF relation, equation 15. (c) The contribution to σ_η from intrinsic scatter and photometric errors. The remainder comes from the δv_{TF} term according to equation 14. (d) The likelihood statistic is scaled by the ratio of the number of independent (237) to total (341) data points in the fit (see §5.1). (e) The x_t -dependence of the TF relation is not modeled, i.e., γ is held fixed at zero. (f) To facilitate comparison with the f_s -formulation, δv_{TF} is held fixed at 15.95 km s^{-1} .

panel), further underscores this point. Although there is a correlation of x_t with luminosity, it is not a tight one. There is, perhaps surprisingly, no correlation between RC shape and surface brightness at all. Galaxies with given luminous properties can have a wide range of RC shapes, and vice versa. Unless the RC shape is accounted for, via the parameter x_t , luminosity cannot be expected to predict the RC amplitude at large radii.

5.9. A Radius-based TF Relation: the Spiral FP

The multiparameter TF relations discussed above are reminiscent of the FP for elliptical galaxies (cf. §2). The latter, however, usually take the defining structural parameters to be galaxy size, surface brightness, and velocity width; here we have stayed closer to the TF relation and used luminosity in preference to size. These formulations are not independent, since luminosity $\propto I_e r_e^2$. Thus, our TF relation $v_{\text{TF}} \propto L^{0.28} I_e^{0.14}$ implies $v_{\text{TF}} \propto I_e^{0.42} r_e^{0.56}$. Solving for r_e this yields $r_e \propto v_{\text{TF}}^{1.79} I_e^{-0.75}$. One may compare this with the elliptical FP relation (e.g., Jorgensen *et al.* 1996) $r_e \propto \sigma^{1.24} I_e^{-0.77}$. The velocity width dependence is significantly stronger for the spirals, but the surface brightness dependence very similar.

The above result assumes $L \propto I_e r_e^2$, which may not be precisely true. In contrast to the procedure generally used with ellipticals, in the LP10K data set luminosity is derived independently from I_e and r_e . Furthermore, the multiparameter TF fits above included the variables f_s and c , and it is not a priori obvious that they should enter the $v_{\text{TF}}-r_e-I_e$ relation in the same way. It is thus worthwhile to fit a standard FP relation directly to the data. We

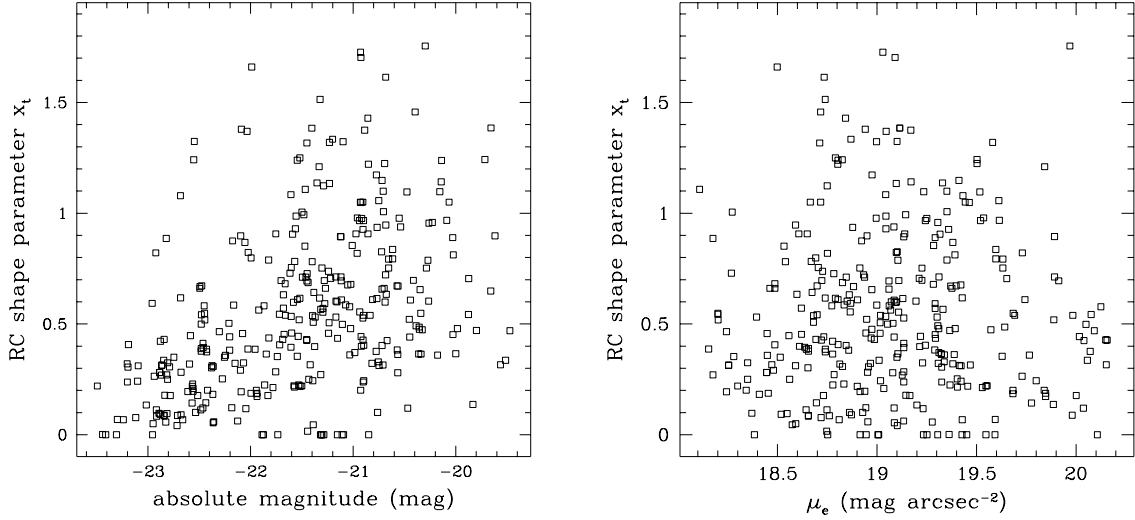


Fig. 8.— The RC shape parameter x_t plotted against absolute magnitude (left) and effective surface brightness (right). There is a trend of x_t with luminosity, in the sense that higher-luminosity objects have smaller values of x_t in the mean, but the trend is not at all a tight one. No meaningful trend of x_t with surface brightness can be seen.

do so by writing

$$\eta = s(\log R_e - T) - \alpha\mu_e + \beta c, \quad (16)$$

where η is derived from v_{TF} as in §5.3. In equation 16, R_e is the absolute diameter, in kpc, corresponding to the observed angular diameter r_e . Distance is derived from a pure Hubble flow model as before.

The results of carrying out such a fit are presented in Table 4; for simplicity, the TF scatter was treated as a constant for the fit. The fit parameters imply a spiral FP of the form $v_{\text{TF}} \propto R_e^{0.51} I_e^{0.39}$, or $R_e \propto v_{\text{TF}}^{1.96} I_e^{0.76}$. Again, the surface brightness exponent is quite similar to the elliptical case, but the velocity dependence is significantly stronger. It is noteworthy that the best fit value of f_s is 2.05, identical within errors to what was obtained from the luminosity-based fit. We may conclude that the radius-based fit and the luminosity-based fit reflect roughly the same physical properties of the galaxies. However, the likelihood statistic is considerably worse, and the TF scatter higher, for the radius-based fit than for the luminosity-based fit (the appropriate comparison is with the third row of Table 2). Evidently R_e is not as good an indicator of rotation velocity as luminosity. This reduces its utility as a distance indicator. In future papers in this series, the luminosity fit will be used in preference to the radius-based fit.

TABLE 4
TF FIT PARAMETERS: RADIUS-BASED FP^a

T	s	α	β	f_s^b	σ_η^c	\mathcal{L}^d
0.537	0.513	0.157	0.076	2.055	0.0644	−1079.5

Table 4: Notes: (a) The parameters T , s , α , and β are defined by equation 16, where R_e is measured in kpc. (b) The parameter f_s has the same meaning here as described in the notes to Table 2. (c) TF scatter treated as a constant. (d) The likelihood statistic is scaled by the ratio of the number of independent (245) to total (352) data points in the fit (see §5.1).

6. Discussion

In this paper several key features of the TF relation have been identified. The first is that the TF relation is optimized—its scatter is minimized—when v_{TF} is taken as the amplitude of the rotation curve at about two disk scale lengths (cf. Figure 2). This would not have been the case if spiral RCs possessed “universal” properties, as has been advocated by Persic, Salucci, & Stel (1996; PSS96). Under the PSS96 hypothesis, it is not merely the amplitude but the entire RC that is specified by luminosity: $v(r) = v_0(L)f(x; L)$, where $x = r/R_{\text{opt}}$ and R_{opt} is a characteristic optical radius. Were this so, the radius at which one chooses to evaluate the RC amplitude should be irrelevant, provided it is the same multiple of the optical radius⁴ for all galaxies. Here we have affirmed the conclusions of Courteau (1997), Kasen (1997), and Simon (1998), that there is something special about the RC amplitude at two disk scale lengths as regards the TF relation. Luminosity is a poor predictor of the value of the RC at very small and very large radii.

This result implies that RCs are *not* universal. Galaxies of a given luminosity can have RCs of very different shapes. This is exemplified by Figure 8, which shows that the RC shape parameter x_t is only loosely correlated with luminosity (and not at all with surface brightness). High-luminosity galaxies are more likely to have classical, flat RCs ($x_t \ll 1$) than are low-luminosity ones, but some high-luminosity galaxies have slowly rising RCs. Low luminosity-spirals are more likely to have quasi-linear RCs ($x_t \gtrsim 1$), but some in fact have flat RCs. This is why one must evaluate TF rotation velocity, v_{TF} , at a particular radius, defined by the surface brightness profile, to obtain a strong correlation with luminosity.

A corollary is that the asymptotic or flat value of the RC, v_a , is not well correlated with

⁴While PSS96 use a radius R_{opt} defined by a fixed fraction of enclosed light, we have used a characteristic radius r_e here. However, the two are linearly related with relatively little scatter and thus the distinction is unimportant.

luminosity, as shown especially well by Figure 7. If the RC rises slowly within the luminous disk ($x_t \gtrsim 1$), the luminosity underpredicts v_a . In order to use v_a as the TF velocity, one must explicitly incorporate the shape parameter x_t into the TF relation, as in Eq. 15. The resultant TF relation exhibits scatter as small as that obtained by taking v_{TF} as the RC amplitude at two scale lengths.

The fact that TF scatter is minimized when v_{TF} is taken as the RC amplitude at two disk scale lengths has important implications for the dark halos of spiral galaxies. Let us assume that spirals consist of a thin disk of mass surface density $\Sigma(r) = \Sigma_0 e^{-r/R_d}$, and a spherical dark halo with a density profile $\rho(r) = \rho_h \chi(r/R_h)$. Here, ρ_h is a generic “central density” of the halo (not necessarily the density at $r = 0$, which is infinite in some models), and R_h a generic scale length (we consider a specific model for the dimensionless density profile $\chi(r/R_h)$ below). One can then show (Dorris & Willick 1998) that the rotation velocity at radius r may be written

$$v_c^2(x) = 4\pi G \Sigma_0 R_d \left[\kappa(x) + \gamma \alpha^{-1} \epsilon(x/\alpha) \right], \quad (17)$$

where:

$$x \equiv \frac{r}{R_d}, \quad (18)$$

$$\kappa(x) = \frac{x^2}{4} \left[I_0\left(\frac{x}{2}\right) K_0\left(\frac{x}{2}\right) - I_1\left(\frac{x}{2}\right) K_1\left(\frac{x}{2}\right) \right], \quad (19)$$

where I and K are Bessel functions of the first and second kinds,

$$\gamma \equiv \frac{\rho_0 R_h^3}{\Sigma_0 R_d^2}, \quad (20)$$

$$\alpha \equiv \frac{R_h}{R_d}, \quad (21)$$

and the function $\epsilon(x/\alpha)$ is defined by

$$\epsilon(y) = \frac{1}{y} \int_0^y x^2 \chi(x) dx. \quad (22)$$

Note that γ is, to within factors of order unity, the ratio of halo to disk mass, while α measures the relative sizes of the two components.

It is evident from Equation 17 that, if α and γ had “universal” values—if dark halos were always the same mass and size relative to the luminous disks which inhabit them—circular velocity would be a function of $x = r/R_d$ alone. If that were the case one could take v_{TF} to be the amplitude of the RC at any multiple of the disk scale length, without changing the accuracy of the TF relation. A plausible explanation for the TF scatter being minimized at

$x \simeq 2$ is that the halo parameters ρ_0 and R_h vary for disks of a given mass and scale length and thus that α and γ are not constant.

We can quantify this idea further as follows. Suppose that halos vary, but in a predictable way, such that γ is a function of α (i.e., central density is a function of physical size, or mass), as expected from theories of hierarchical structure formation (e.g., Navarro, Frenk, & White 1996, hereafter NFW). Then from Eq. 17 one can show that variation in $\ln v_c$ due to changes $\delta\alpha$ in halo size is

$$\delta \ln v_c(x) = \frac{v_h^2(x)}{2v_c^2(x)} \left[\frac{d \ln \gamma}{d \ln \alpha} - \left(1 + \frac{d \ln \epsilon}{d \ln z} \Big|_{z=x/\alpha} \right) \right] \frac{\delta \alpha}{\alpha}, \quad (23)$$

where $v_h^2 = 4\pi G \rho_0 R_h^2 \epsilon(x/\alpha)$ is the rotation speed due to the halo alone. If indeed the TF scatter minimizes at $x = 2$ because halo mass and size variations have no effect there, by Equation 23 it follows that

$$\frac{d \ln \gamma}{d \ln \alpha} = 1 + \frac{d \ln \epsilon}{d \ln z} \Big|_{z=2/\alpha} \quad (24)$$

This represents a constraint on the properties of the dark halo. If this constraint is satisfied, halo mass and size variations will not affect the scatter of the TF relation when v_{TF} is taken at $r = 2R_d$. On the other hand, if Equation 24 is satisfied, then at some other radius x the RC amplitude variation due to halo mass and size variations will, according to Equation 23, be given by

$$\delta \ln v_c = \frac{v_h^2}{2v_c^2} \left[\frac{d \ln \epsilon(z)}{d \ln z} \Big|_{z=2/\alpha} - \frac{d \ln \epsilon(z)}{d \ln z} \Big|_{z=x/\alpha} \right] \frac{\delta \alpha}{\alpha}. \quad (25)$$

As a concrete example, let us suppose that the halo mass distribution is given by the model proposed by NFW,

$$\rho_{\text{NFW}}(r) = \rho_0 \left(\frac{r}{R_h} \right)^{-1} \left(1 + \frac{r}{R_h} \right)^{-2}. \quad (26)$$

Using $\rho_{\text{NFW}}(r)$ in Equation 22 we find

$$\frac{d \ln \epsilon(z)}{d \ln z} = \frac{z^2/(1+z^2)}{\ln(1+z) - z/(1+z)} - 1. \quad (27)$$

Before using this formula, we must adopt a suitable value of α . The requirement that RCs be well-approximated by an arctangent shape constrains α to lie in the range ~ 7 – 12 for luminous disks within NFW halos (Dorris & Willick 1998). We adopt $\alpha = 10$ for this discussion; the conclusions are not sensitive to its precise value. We then find that $(d \ln \epsilon / d \ln z)_{z=2/\alpha} = 0.78$. If we consider only luminous disks of fixed mass and size,

$d \ln \gamma / d \ln \alpha = d \ln M_h / d \ln R_h$. If we further assume $\rho_h \propto R_h^{-\beta}$, the constraint Eq. 24 implies $\rho_h \propto R_h^{-1.2}$, or, equivalently, $\rho_h \propto M_h^{-0.7}$. Thus, the TF scatter minimum when v_{TF} is taken at two scale lengths, along with several additional assumptions, implies a particular scaling of halo central density with halo mass. The indicated scaling is consistent with the predictions of hierarchical structure formation scenarios, although a rather flat power spectrum ($n \gtrsim -1.5$) on galaxy halo scales would be required (see Figure 9 of NFW).

If we then use Equation 27 in Equation 25, take $x = 5$ (where we assume the RC is halo-dominated), and assume that typical variations in α are 50%, we find that $\delta \ln v_c(x = 5) \simeq 0.08$, corresponding to $\delta \eta \simeq 0.034$. Such an error, added in quadrature with a minimum error $\sigma_\eta \simeq 0.06$, yields $\sigma_\eta = 0.069$. This is quite comparable to what is shown in Figure 2 as we go from $f_s = 2$ to $f_s = 5$. Thus, reasonable variations in halo mass at fixed disk mass can account for the increase in TF scatter when v_{TF} is taken as the asymptotic RC amplitude.

The preceding argument is illustrative only. The NFW profile may not describe low-surface brightness spirals well (Kravtsov *et al.* 1998), and we have neglected the effect of a bulge component altogether, which is certainly important at small x . Nonetheless, the main point of the argument remains valid: if spirals of a given mass and size can be found within dark halos of variable mass and size, this will, in general, contribute to the TF scatter when v_{TF} is taken at an arbitrary radius. However, if the halos exhibit a well-defined mass-size relationship, as embodied in Equation 24, this contribution to the TF scatter will vanish when v_{TF} is taken as the RC amplitude at two disk scale lengths. A detailed consideration of these issues will be presented in a forthcoming paper (Dorris & Willick 1998).

A second important result of this paper has been that the TF relation is not a two parameter relation. The $v_{\text{TF}}-L$ relation exhibits residuals that correlate, though weakly, with surface brightness (upper panel of Figure 3). When SB is incorporated into the relation one obtains a significant reduction in scatter and improvement in likelihood of the fit. The best-fit TF relation may be written $v_{\text{TF}} \propto L^{0.28} I_e^{0.14}$, where I_e is effective central surface brightness (cf. Appendix A). If we neglect mass-to-light variations, (i.e., if we assume mass is proportional to luminosity and surface density is proportional to surface brightness) then Eq. 17 reduces to $v_{\text{TF}} \propto L^{0.25} I_e^{0.25}$. The observed TF relation is very close to this virial prediction in terms of the luminosity-dependence, but the surface brightness dependence is significantly weaker. Nonetheless, the existence of an SB-dependence is important. It has generally been assumed that the TF relation lacks such a dependence, and this has been explained in the past as a consequence of the dark halo dominating the mass within 2 scale lengths and masking the SB dependence (Courteau & Rix 1999; McGaugh & de Blok 1998, Navarro 1998) The detection here of a significant SB dependence of the TF relation shows that the virial theorem is approximately, though not precisely, obeyed within two

scale lengths. The halo may conspire to reduce the SB dependence, but it does not eliminate it altogether, which requires less fine-tuning to explain. Alternatively, the sub-virial SB dependence could be a consequence of a mild decrease in mass-to-light ratio with increasing surface brightness. Which if either of these possibilities holds is not clear; the problem deserves further study.

A related conclusion we may draw from this result is that the properties of spirals are closer to those of ellipticals, which exhibit fundamental plane relations, than has previously been appreciated. This conclusion has been anticipated in the work of Bender, Burstein, Faber, & Nolthenius (1997), who have emphasized that all galaxies — indeed all gravitationally bound stellar systems—inherit a fundamental plane, the “cosmic metaplane.” However, Bender *et al.* considered the two-dimensional, $v_{\text{TF}}-L$, locus in parameter space, to represent the FP of spirals. The SB-dependence of the TF relation shows that the FP of spirals is not parallel to the $v_{\text{TF}}-L$ plane. We have also shown that the spiral data may be fitted directly to the elliptical FP variables (radius, velocity, and surface brightness), yielding the result $R_e \propto v_{\text{TF}}^{1.84} I_e^{0.76}$. The I_e exponent is very similar to what has been found for ellipticals, though the v_{TF} exponent is significantly larger. However, we found that the FP defined by v_{TF} , $\log R_e$, and I_e (the “radius-based” FP) exhibits noticeably larger scatter than the $v_{\text{TF}}-L-I_e$ fit (the “luminosity-based” FP). In this sense, spirals hew more closely to the traditional TF relation than to the FP of ellipticals. This may well be related to the fact that, because of their relatively sharp edges, it is easier to measure the total luminosity of spirals than it is for ellipticals.

A final comment concerns the dependence on concentration index, c , found here for both the luminosity and radius-based spiral FPs. This is probably not a fundamental consideration. Rather, the presence of c probably serves mainly to correct the effective radius r_e for galaxies of different luminosity profiles. Its effect is significant only for highly concentrated galaxies. These are objects with strong bulges for which r_e , which is relatively insensitive to the innermost SB profile, overstates the spatial extent of luminous mass. The concentration index dependence of the TF relation represents a small correction for this effect.

7. Summary

We have presented the first results from the Las Campanas-Palomar 10,000 km s^{-1} (LP10K) cluster survey. The survey includes TF data for spirals and FP data for ellipticals found within ~ 1 deg of the centers of 15 Abell clusters. The elliptical galaxy observations and analysis are ongoing; this paper, along with Papers II and III, concerns the TF results only. The principal aim of the LP10K survey is to constrain bulk peculiar velocities on very

large ($\gtrsim 100h^{-1}$ Mpc) scales.

The LP10K TF data set is one of a number of recent TF surveys based on rotation curves measured from long-slit spectroscopy. We may now ask, how can we use the full information contained in the RC—and not just a single “velocity width”—to optimize the TF relation? Another relevant question is how best to use detailed surface photometric information derived from CCD imaging in TF analyses. The focus of this paper has been to address these and related issues using the LP10K TF data set, and to interpret the results in light of plausible models of spiral galaxy structure.

Several key parameters were derived from the photometric and spectroscopic data. In addition to an R -band apparent magnitude, the surface brightness profile was used to calculate an effective exponential radius r_e and central surface brightness I_e . These parameters were determined from intensity moments (Appendix A) rather than from a direct fit to the profile, and thus are robust and objective. A luminosity concentration index c was also computed from the surface photometry profile. The long-slit spectroscopy produced a rotation curve $v_c(r)$ measured from the $\text{H}\alpha$ emission line. The RCs were fitted by a two-parameter arctangent function (Equation 3), an adequate fit in all cases. This procedure yielded an RC turnover radius r_t and asymptotic velocity v_a . We define $x_t = r_t/r_e$, the ratio of the dynamical to luminous scale length of the galaxy. Objects with $x_t \ll 1$ exhibit classical rotation curves with a flat or nearly flat portion. Objects with $x_t \gtrsim 1$ have slowly rising RCs that may not flatten out within the measured region.

We carried out a series of maximum-likelihood fits of the inverse TF relation, essentially minimizing residuals of the circular velocity parameter $\eta = \log v_{\text{TF}} - 2.5$. The TF rotation velocity v_{TF} was obtained from the arctangent fit:

$$v_{\text{TF}} = \frac{2v_a}{\pi} \tan^{-1} \left(\frac{f_s r_e}{r_t} \right) = \frac{2v_a}{\pi} \tan^{-1} \left(\frac{f_s}{x_t} \right). \quad (28)$$

The quantity f_s was treated as a free parameter to be determined via likelihood maximization. The fits were optimized for $f_s = 2.0 \pm 0.2$. This conclusion confirms that reached earlier by Courteau (1997), Kasen (1997), and Simon (1998). These studies indicate that v_{TF} must be referenced to the luminosity structure of the galaxy, not taken from the asymptotically flat part of the RC; only when $x_t \ll 1$ are v_{TF} and v_a effectively equivalent. This finding is at variance with the conventional wisdom concerning the TF relation, which holds that it is the amplitude of the flat portion of the RC which best correlates with luminosity (e.g., McGaugh & de Blok 1998). A corollary is that spirals cannot be characterized in terms of a “universal” rotation curve (URC), as has been argued by Persic, Salucci, & Stel (1996). The URC hypothesis holds that luminosity uniquely specifies not only RC amplitude, but also the entire functional form of the RC. Were this the case, one should be able to evaluate v_{TF}

and any chosen multiple of the effective radius r_e , and obtain an equally tight TF relation. As Figure 2 clearly shows, this is not the case.

The physical mechanism most likely responsible for the TF optimization at two scale lengths is variation in the mass and size of the dark halos in which galaxies of given luminous mass and size reside. A simple model was presented (§6) to demonstrate the outlines of this effect. If a spherical dark halo of central density ρ_h and scale length R_h surrounds a disk galaxy, variations in ρ_h and R_h will affect its contribution to the RC at all radii. However, these effects will cancel at $r = 2r_e$, provided that ρ_h varies with R_h in the manner predicted by equation 24. This constraint is dependent on the specific model of the halo one adopts. For an NFW halo whose parameters are tuned to yield reasonable RC shapes, the constraint may be stated $\rho_h \propto M_h^{-0.7}$, where M_h is the total mass of the halo. Such a result is roughly consistent with the mass-density relation derived from numerical simulations of structure formation (NFW).

We have also demonstrated that TF residuals from a standard two-parameter fit, $v_{\text{TF}} \propto L^\alpha$, are correlated, albeit weakly, with surface brightness. A tighter TF relation is obtained if SB is explicitly incorporated into the fit. The resultant three-parameter TF relation may be written $v_{\text{TF}} \propto L^{0.28} I_e^{0.14}$. Such a TF relation resembles the fundamental plane of elliptical galaxies more closely than does the standard two-parameter relation, and indeed is closer to the prediction from simple virial equilibrium considerations. However, the surface-brightness dependence remains sub-virial, a result still in need of explanation.

We found a significant decrease in the TF scatter with increasing luminosity and surface brightness. We suggested that this effect follows naturally if rotation velocity measurement errors, δv_{TF} , are independent of v_{TF} itself, so that $\delta \ln v_{\text{TF}} \propto v_{\text{TF}}^{-1}$. Incorporating this model improves the fit likelihood and suggests that typical rotation velocity measurement errors are $\sim 15 \text{ km s}^{-1}$. These errors dominate the TF scatter for slow rotators ($v_{\text{TF}} \lesssim 150 \text{ km s}^{-1}$), while for rapid rotators—high luminosity, high-SB galaxies—the intrinsic scatter of the TF relation, $\lesssim 0.30 \text{ mag}$, dominates the observed scatter.

The above properties of the TF relation will be used in subsequent papers in this series, which will investigate deviations from uniform Hubble flow using the LP10K sample.

The author acknowledges the support of NSF grant AST-9617188 and the Research Corporation.

REFERENCES

Aaronson, M., Huchra, J., Mould, J., Schechter, P. L., & Tully, R. B. 1982, *ApJ*, 258, 64

Aaronson, M., Bothun, G., Mould, J., Huchra, J., Schommer, R.A., and Cornell, M.E. 1986, *ApJ*, 302, 536

Bender, R., Burstein, D., & Faber, S.M. 1992, *ApJ*, 399, 462

Bottinelli, L., Gouguenheim, L., Paturel, G., & de Vaucouleurs, G. 1983, *A&A*, 118, 4

Courteau, S. 1992, PhD. Thesis, University of California, Santa Cruz

Courteau, S., Faber, S.M., Dressler, A., & Willick, J.A. 1993, *ApJ*, 412, L51

Courteau, S. 1997, *AJ*, 114, 2402

Courteau, S., & Rix, H.-W. 1999, *ApJ*, in press (astro-ph/9707290)

Courteau, S., Willick, J.A., Schlegel, D., Strauss, M.A., & Postman, M. 1998, in preparation (SHELLFLOW)

Dekel, A. 1994, *ARA&A*, 32, 371

Djorgovski, S., & Davis, M. 1987, *ApJ*, 313, 59

Dorris, M., & Willick, J.A. 1998, in preparation

Dressler, A., Faber, S.M., D., Burstein, D., Davies, R.L., Lynden-Bell, D., Terlevich, R.J., and Wegner, G. 1987, *ApJ*, 313, L37

Giovanelli, R., Haynes, M.P., Wegner, G., da Costa, L.N., Freudling, W., & Salzer, J.J. 1996, *ApJ*, 464, L99

Han, M.-S. 1991, PhD. Thesis, California Institute of Technology

Han, M.-S., & Mould, J.R. 1992, *ApJ*, 396, 453

Jarvis, J.F., & Tyson, J.A. 1981, *AJ*, 86, 476

Jorgensen, I., Franx, M., & Kjaergaard, P. 1996, *MNRAS*, 280, 167

Kasen, D. 1997, unpublished undergraduate thesis, Stanford University
<http://astro.stanford.edu/jeffw/ugthesis>

Kravtsov, A.V, Klypin, A.A., Bullock, J.S., & Primack, J.R. 1998, *ApJ*, 502, 48

Landolt, A.U. 1992, AJ, 104, 340

Lauer, T.R., & Postman, M. 1994, ApJ, 425, 418

Mathewson, D. S., Ford, V. L., & Buchhorn, M. 1992, ApJS, 81, 413

McGaugh, S.S., & de Blok, W.J.G. 1998, ApJ, 499, 41

Navarro, J.F., Frenk, C.S., & White, S.D.M. 1997, ApJ, 490, 493 (NFW)

Navarro, J.F. 1998, preprint (astro-ph/9807084)

Persic, M, Salucci, P., & Stel, F. 1996, MNRAS, 281, 27

Pierce, M.J., and Tully, R.B. 1988, ApJ, 330, 579

Postman, M. 1995, in *Dark Matter*, Proceedings of the 5th Maryland Astrophysics Conference, AIP Conference Series 336, 371

Riess, A.G., Davis, M., Baker, J., & Kirshner, R.P. 1997, ApJ, 488, L1

Rubin, V.C., Ford, W.K., Thonnard, N., & Burstein, D. 1982, ApJ, 261, 439

Schlegel, D. 1995, PhD. Thesis, University of California, Berkeley

Schlegel, D., Finkbeiner, D.P., & Davis, M. 1998, ApJ, 500, 525

Simon, J. 1998, unpublished undergraduate thesis, Stanford University
<http://astro.stanford.edu/jeffw/ugthesis>

Stover, R.J. 1988, in *Instrumentation for Ground-Based Optical Astronomy, Present and Future*, L.B. Robinson, Ed. (New York: Springer-Verlag)

Strauss, M.A., Cen, R., Ostriker, J.P., Lauer, T.R., & Postman, M. 1995, ApJ, 444, 507

Strauss, M. A., & Willick, J. A. 1995, Phys. Rep., 261, 271

Strauss, M. A. 1997, in Critical Dialogues in Cosmology, ed. N. Turok (Singapore: World Scientific), 423

Tully, R.B., & Fisher, J.R. 1977, A&A, 54, 661

Willick, J. A. 1991, PhD. Thesis, University of California, Berkeley

Willick, J. A., Courteau, S., Faber, S. M., Burstein, D., & Dekel, A. 1995, ApJ, 446, 12

Willick, J. A., Courteau, S., Faber, S. M., Burstein, D., Dekel, A., & Kolatt, T. 1996, ApJ, 457, 460

Willick, J. A., Courteau, S., Faber, S. M., Burstein, D., Dekel, A., & Strauss, M. A. 1997a, ApJS, 109, 333

Willick, J. A., Strauss, M. A., Dekel, A., & Kolatt, T. 1997b, ApJ, 486, 629

Willick, J. A., & Strauss, M. A. 1998, ApJ, in press (astro-ph/9801307)

Willick, J. A. 1998a, in preparation (Paper II)

Willick, J. A. 1998b, in preparation (Paper III)

Willick, J. A. 1998c, in *Formation of Structure in the Universe*, eds. A. Dekel & J. P. Ostriker (Cambridge Univ. Press), in press

A. Characteristic Surface Brightness and Scale from Moments of the Intensity Distribution

It is customary to model spiral galaxy intensity profiles as exponential, $I(r) = I_0 e^{-r/r_d}$. The central intensity I_0 and the disk scale length r_d then provide convenient measures of surface brightness and radius. For two reasons, however, it is not optimal to obtain these quantities by fitting exponential functions to the observed intensity profile. First, many real spirals are not accurately exponential. Second, any fitting of a profile is necessarily subjective: a start and end point for the fit must be selected, particular points may be rejected, etc. Different choices will yield different values of I_0 and of r_d .

For these reasons, an objective measurement of characteristic surface brightness and scale—one that does not rely on a fit—is needed. However, given that many spirals are approximately exponential, it is desirable that the objective approach recover the exponential parameters in the event that the galaxy is, in fact, accurately exponential. When it is not, the approach should still produce well-defined and sensible measures of surface brightness and scale. Such a method is described in what follows.

Given an intensity profile $I(r)$ measured to a maximum radius r_f , define the n -th moment of the intensity distribution by

$$f_n = \int_0^{r_f} r^n I(r) dr. \quad (\text{A1})$$

The moments f_n are readily computed from the measured surface brightness profile, usually by taking $I(r)$ as the median surface brightness measured on an elliptical isophote of major axis radius r .

If $I(r)$ is indeed exponential with central intensity I_0 and scale length r_d , then the moments are given by

$$f_n = I_0 \int_0^{r_f} r^n e^{-r/r_d} dr = I_0 r_f^{n+1} h_n(y_f), \quad (\text{A2})$$

where $y_f \equiv r_f/r_d$, and the dimensionless functions h_n are defined by

$$h_n(y) = \frac{1}{y^{n+1}} \int_0^y x^n e^{-x} dx. \quad (\text{A3})$$

From equation A2 we find that, for an exponential profile,

$$\frac{1}{r_f^2} \frac{f_3}{f_1} = \frac{h_3(y_f)}{h_1(y_f)} = \frac{1}{y_f^2} \frac{6 - e^{-y_f}(6 + 6y_f + 3y_f^2 + y_f^3)}{1 - e^{-y_f}(1 + y_f)}, \quad (\text{A4})$$

where in the last step the integrals have been explicitly evaluated. From equation A2 we also find that, for an exponential profile

$$I_0 = \frac{f_2}{r_f^3 h_2(y_f)}. \quad (\text{A5})$$

Equation A4 is a transcendental equation for y_f in terms of the observables r_f , f_1 , and f_3 that may be solved using standard numerical techniques. Having obtained y_f in this way, one calculates the exponential scale length $r_d = r_f/y_f$. The central surface brightness I_0 is then obtained by substituting y_f into equation A5.

This procedure has been tested on simulated galaxy profiles. When the profiles are exponential, it recovers accurately the true central intensity I_0 and exponential scale length r_d . However, the procedure is perfectly well-defined for well-behaved but otherwise arbitrary intensity profiles as well. In particular, one may always calculate y_f from equation A4, and then *define* an effective radius $r_e = r_f/y_f$ and an effective central surface brightness $I_e = f_2/[r_f^3 h_2(y_f)]$. These effective quantities are objective and robust against irregularities in the profile. Most importantly, they are, as discussed in the main body of the paper, found to be suitable measures of radius and surface brightness in the TF relation.